1-28-2014

Pulsed, Cross-Shelf Export of Terrigenous Dissolved Organic Carbon to the Gulf of Mexico

Cedric Fichot
University of South Carolina - Columbia

Steven E. Lohrenz
School for Marine Science and Technology

Ronald Benner
University of South Carolina - Columbia, benner@mailbox.sc.edu

Publication Info

Published in *Journal of Geophysical Research: Oceans*, Volume 119, Issue 2, 2014, pages 1176-1194.

2014

The fate of terrigenous dissolved organic carbon in a river-influenced ocean margin

Ronald Benner

Cedric Fichot

AGU PUBLICATIONS

JGR

Journal of Geophysical Research: Oceans

RESEARCH ARTICLE

10.1002/2013JC009424

Key Points:
- Surface tDOC concentrations are retrieved using ocean-color remote sensing
- tDOC cross-shelf export is sporadic and exhibits large interannual variability
- tDOC cross-shelf export is enhanced during years of anomalously high discharge

Correspondence to:
C. G. Fichot,
cgfichot@gmail.com

Citation:
Fichot, C. G., S. E. Lohrenz, and R. Benner (2014), Pulsed, cross-shelf export of terrigenous dissolved organic carbon to the Gulf of Mexico, *J. Geophys. Res. Oceans*, *119*, doi:10.1002/2013JC009424.

Received 10 SEP 2013
Accepted 18 JAN 2014
Accepted article online 28 JAN 2014

Pulsed, cross-shelf export of terrigenous dissolved organic carbon to the Gulf of Mexico

Cédric G. Fichot[1,2], Steven E. Lohrenz[3], and Ronald Benner[1,2]

[1]Marine Science Program, University of South Carolina, Columbia, South Carolina, USA, [2]Department of Biological Sciences, University of South Carolina, Columbia, South Carolina, USA, [3]Department of Estuarine and Ocean Sciences, School for Marine Science and Technology, University of Massachusetts, Dartmouth, Massachusetts, USA

Abstract The export of terrigenous dissolved organic carbon (tDOC) and other river-borne material across the continental shelf boundary has important ramifications for biological productivity and the cycling of continentally derived bioelements in the ocean. Recent studies revealed the 275–295 nm spectral slope coefficient of chromophoric dissolved organic matter (CDOM), $S_{275-295}$, is a reliable tracer for terrigenous dissolved organic carbon (tDOC) in river-influenced ocean margins. Here an empirical algorithm for the accurate retrieval of $S_{275-295}$ from ocean color was developed and validated using in situ optical properties collected seasonally in the northern Gulf of Mexico. This study also demonstrated $S_{275-295}$ is a robust proxy for tDOC concentration in this environment, thereby providing a means to derive surface tDOC concentrations on synoptic scales and in quasi-real time using remote sensing. The resulting tDOC-algorithm was implemented using *Aqua*-MODIS in a retrospective analysis of surface tDOC concentrations over the northern Gulf of Mexico between July 2002 and June 2013. Large pulses of tDOC were observed in continental-slope surface waters off the Mississippi River delta, indicating cross-shelf export of tDOC was sporadic and exhibited considerable interannual variability. Favorable winds following an anomalously high discharge from the Mississippi-Atchafalaya river system always coincided with a major export event, and in general, cross-shelf export was enhanced during years of anomalously high discharge. The tDOC-algorithm will find applicability in the assessment of future climate- and human-induced changes in tDOC export, in biogeochemical models of the continental shelf, and in the validation of high-resolution coastal models of buoyancy-driven shelf circulation.

1. Introduction

Rivers discharge ~0.25 Pg of tDOC to the global ocean each year, and it appears most of this material is mineralized in ocean margins [*Hedges et al*., 1997; *Opsahl and Benner*, 1997; *Bianchi*, 2011; C. G. Fichot and R. Benner, The fate of terrigenous dissolved organic carbon in a river-influenced ocean margin, submitted to *Global Biogeochemical* Cycles, 2014]. Nevertheless, measurable amounts of dissolved lignin throughout the global ocean indicate some tDOC escapes mineralization on continental shelves and is exported to the open ocean [*Meyers-Schulte and Hedges*, 1986; *Hernes and Benner*, 2002; *Dittmar and Kattner*, 2003; *Benner et al*., 2005]. The cross-shelf export of tDOC and its subsequent microbial and photochemical processing can influence the net metabolic state and air-sea CO_2 balance of these environments by nutrient enhancement of primary production and by directly fueling microbial respiration [*Smith and Hollibaugh*, 1993]. Furthermore, tDOC export is often associated with riverine transport of trace metals, pollutants, and pathogens to marine ecosystems. Despite its importance, the influence of tDOC and other riverine materials beyond the continental shelf remains poorly understood, as the current quantitative approaches [*Hedges et al*., 1992; *Dittmar et al*., 2007; *Kaiser and Benner*, 2012] cannot be practically applied to trace tDOC over broad temporal and spatial scales.

The spectral slope coefficient of chromophoric dissolved organic matter (CDOM) between 275 and 295 nm ($S_{275-295}$) [*Helms et al*., 2008] was recently established as a reliable optical tracer for tDOC in river-influenced ocean margins [*Fichot and Benner*, 2012], and its amenability to remote sensing of ocean color has been demonstrated in the Arctic Ocean [*Fichot et al*., 2013]. Herein, an empirical algorithm for the retrieval of $S_{275-295}$ and tDOC concentrations from ocean color is developed and validated for application in the northern Gulf of Mexico. The algorithm is then implemented using *Aqua*-Moderate Resolution Imaging

Spectroradiometer (MODIS) ocean color in a retrospective analysis (July 2002 to June 2013) of surface tDOC exported across the shelf boundary and into the oceanic waters of the northern Gulf of Mexico. The continental shelf of the northern Gulf of Mexico is influenced by terrigenous inputs from the Mississippi-Atchafalaya River System (M-ARS), and cross-shelf export of M-ARS water to the Gulf of Mexico has been directly observed on several occasions [*Walker et al*., 1996; *Yuan et al*., 2004; *Hu et al*., 2005]. Algorithms for the retrieval of CDOM and/or dissolved organic carbon (DOC) have been developed and used in various applications in this environment [*Hu et al*., 2003; *D'Sa et al*., 2006; *Del Castillo and Miller*, 2008; *Tehrani et al*., 2013] and in other coastal regions [*Hoge et al*., 1995; *Johannessen et al*., 2003; *Mannino et al*., 2008]. The tDOC-algorithm presented here is parameterized specifically to trace DOC derived from land, and thereby provides the means to monitor surface tDOC concentrations on synoptic scales. As such, it will not only shed light on the dynamics (past and future) of tDOC and other riverine materials in oceanic regions of the northern Gulf of Mexico, but will also find applicability in biogeochemical and circulation models of this region.

2. Methods

2.1. Overview of Field Sampling and Measurements

Field samples and measurements were collected as part of the GulfCarbon project (http://ocean.otr.usm.edu/~w301130/research/gulfcarbon_new.htm). Surface water samples for chromophoric dissolved organic matter (CDOM) and dissolved organic carbon (DOC) analyses were collected along a grid of 47–51 stations, during five research cruises conducted in the northern Gulf of Mexico in January, April, July, and October-November 2009 and March 2010 (Figure 1a). During each cruise, samples for dissolved lignin analysis were also collected at 18–23 stations, and optical profiles were acquired at 11–20 stations to calculate in situ hyperspectral remote-sensing reflectance spectra just above the sea surface, $Rrs(\lambda, 0^+)$, in the $\lambda = 350$–700 nm wavelength range (Figures 1b–1f). A total set of 246 CDOM samples, 222 DOC samples, 104 dissolved lignin samples, and 75 $Rrs(\lambda, 0^+)$ measurements was thus collected (Table 1). The samples spanned a salinity range of 0–37, from nutrient-rich riverine waters to oligotrophic marine waters, and were collected during contrasting seasons in terms of surface salinity distribution, surface water temperature, wind conditions, and river discharge (Table 2). This data set is therefore representative of the majority of water types and environmental conditions typically encountered in this river-influenced ocean margin and is ideal for the development of robust relationships and algorithms for time series application.

2.2. DOC Sampling and Analysis

Samples for DOC analysis were gravity filtered from Niskin bottles using precombusted GF/F filters (0.7 μm pore size) and stored frozen (-20°C) immediately after collection in precombusted borosilicate glass vials. DOC analysis was conducted within a month of collection by high temperature combustion using a Shimadzu total organic carbon (TOC) TOC-V analyzer equipped with an autosampler [*Benner and Strom*, 1993]. Blanks were negligible and the coefficient of variation between injections of a given sample was typically $\pm$0.6%. Accuracy and consistency of measured DOC concentrations were checked by analyzing a deep seawater reference standard (University of Miami) every sixth sample.

2.3. CDOM Sampling and Analysis, and Calculation of $S_{275-295}$

Samples for CDOM analysis were gravity filtered from Niskin bottles using Whatman Polycap Aqueous Solution (AS) cartridges (0.2 μm pore size), collected in precombusted borosilicate glass vials, and stored immediately at 4°C until analysis in the laboratory. Absorbance of the samples was measured from $\lambda = 250$ to 800 nm using a Shimadzu ultraviolet (UV)-visible UV-1601 dual-beam spectrophotometer and 10 cm cylindrical quartz cells. For highly absorbing samples, 5 cm cylindrical quartz cells or 1 cm quartz cuvettes were used. An exponential fit of the absorbance spectrum over an optimal spectral range was used to derive an offset value that was subtracted from the absorbance spectrum [*Johannessen and Miller*, 2001; *Fichot and Benner*, 2011]. Absorbance corrected for offset was then converted to Napierian absorption coefficients, $a_g(\lambda)$ (m^{-1}). The dependence of $a_g(\lambda)$ on λ is described using equation (1):

$$a_g(\lambda) = a_g(\lambda_0) \cdot \exp\left(-S_{\lambda_0-\lambda}(\lambda-\lambda_0)\right) \quad (1)$$

where $\lambda_0 < \lambda$ and $S_{\lambda_0-\lambda}$ is the spectral slope coefficient in the λ_0–λ nm spectral range. The spectral slope coefficient between 275 and 295 nm, $S_{275-295}$, was calculated as the slope of the linear regression of ln (a_g

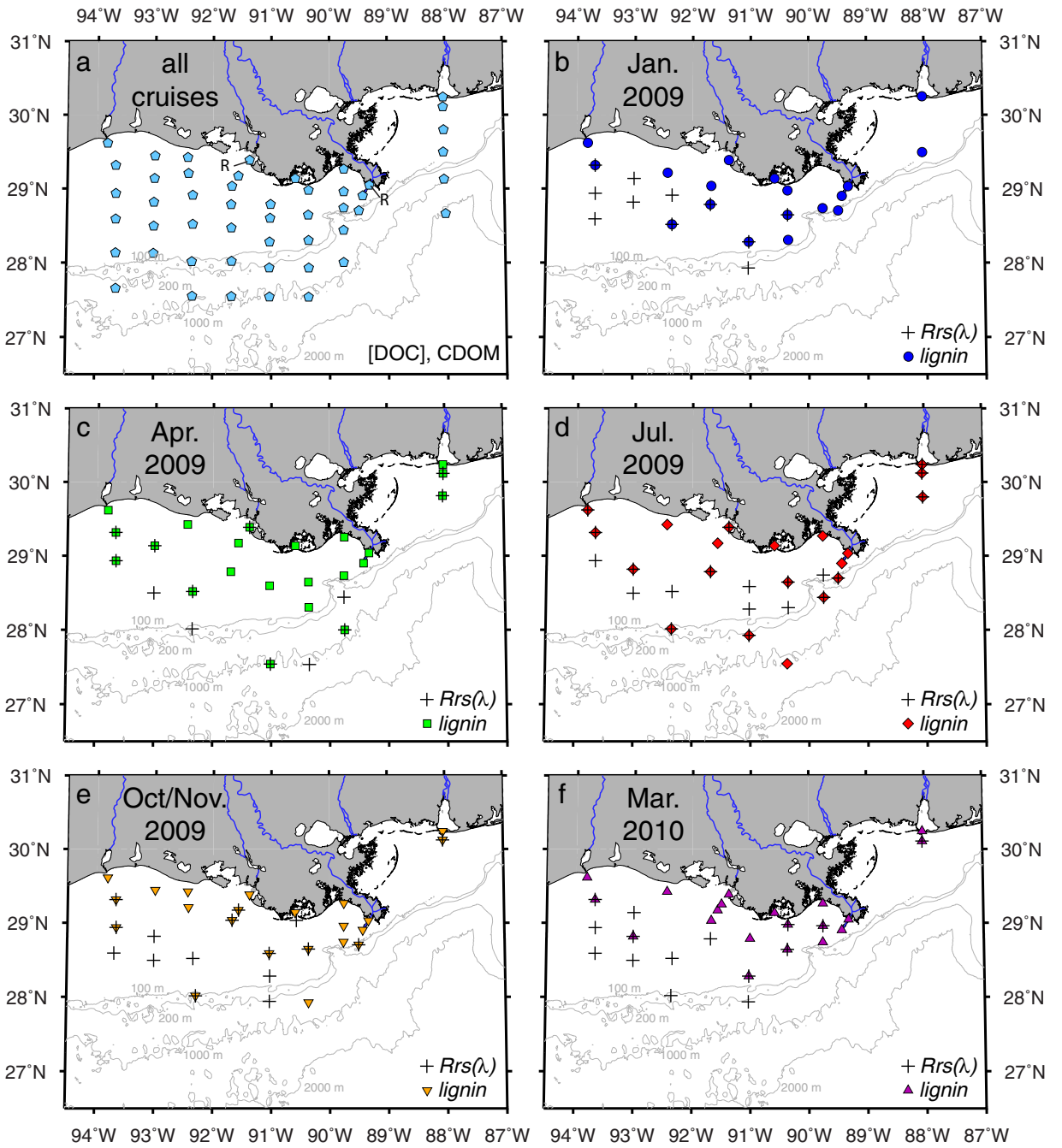

Figure 1. Sampling and field measurement sites in the northern Gulf of Mexico: (a) sampling locations for DOC and CDOM samples collected during all five cruises. Only minor modifications from this sampling grid occured between cruises ($n = 47–51$). The two stations labeled "R" correspond to river stations (salinity = 0). (b–f) Cruise-specific locations of in situ $Rrs(\lambda, 0^+)$ measurements (+ symbols, $n = 11–20$), and cruise-specific sampling sites for dissolved lignin (colored symbols, $n = 18–23$).

(λ)) on λ, between $\lambda = 275$ and 295 nm [*Helms et al.*, 2008; *Fichot and Benner*, 2011]. Here $S_{275–295}$ is reported with units of nm^{-1}.

2.4. Dissolved Lignin Sampling and Analysis, and Calculation of C-Normalized Lignin Yields

Samples for lignin analysis (10 L) were gravity filtered from Niskin bottles using Whatman Polycap AS cartridges (0.2 μm pore size), acidified to pH $\simeq$ 2.5–3 with sulfuric acid, and extracted onboard using C-18

Table 1. General Sampling Information During the Five GulfCarbon Cruises to the Northern Gulf of Mexico[a]

		Number of Samples/Measurements			
Season	Sampling Periods	CDOM ($S_{275-295}$)	[DOC]	Lignin ($TDLP_9$-C)	$Rrs(\lambda,0^+)$
Winter 2009	9–18 Jan 2009	48	24	18	11
Spring 2009	20–30 Apr 2009	50	50	23	13
Summer 2009	19–29 Jul 2009	51	51	21	20
Fall 2009	29 Oct to 7 Nov 2009	47	47	22	16
Winter/spring 2010	11–20 Mar 2010	50	50	20	15
Total		246	222	104	75

[a]Sampling sites are shown in Figure 1.

cartridges [*Louchouarn et al.*, 2000]. Cartridges were stored at 4°C until elution with 30 mL of High-performance liquid chromatography (HPLC)-grade methanol. The elution solutions were then stored at −20°C until analysis. Lignin was analyzed using the CuO oxidation method of *Kaiser and Benner* [2012]. Concentrations of lignin phenols were measured as trimethylsilyl derivatives using an Agilent 7890 gas chromatograph equipped with a Varian DB5-MS capillary column and an Agilent 5975 mass selective detector. The concentrations of nine lignin phenols were measured in this study: *p*-hydroxybenzaldehyde (PAL), *p*-hydroxyacetophenone (PON), *p*-hydroxybenzoic acid (PAD), vanillin (VAL), acetovanillone (VON), vanillic acid (VAD), syringaldehyde (SAL), acetosyringone (SON), and syringic acid (SAD). The sum of nine *p*-hydroxyl, vanillyl, and syringyl lignin phenols ($TDLP_9$) are reported in units of nmol L^{-1}. Corresponding DOC-normalized lignin yields ($TDLP_9$-C) are reported in units of %DOC.

2.5. Field Measurements of $Rrs(\lambda,0^+)$

Hyperspectral remote-sensing reflectance, $Rrs(\lambda, 0^+)$, in the $\lambda = 350$–700 nm wavelength range was derived from simultaneous profiles of hyperspectral downwelling irradiance, $E_d(\lambda, z)$, and upwelling radiance, $L_u(\lambda, z)$, (where z is the depth) acquired using a Satlantic HyperPRO free-falling optical profiler equipped with a surface irradiance reference. The maximum depth of the optical profiles ranged from a few meters in near-shore waters to ~ 50 m in oligotrophic waters. At each sampled station, the measurements of $E_d(\lambda, z)$ and $L_u(\lambda, z)$ collected during three optical profiles in clear, oligotrophic offshore waters and ~20 optical profiles in shallow, turbid waters were pooled together and used to calculate a $Rrs(\lambda, 0^+)$ spectrum as in equation (2)

$$Rrs(\lambda,0^+)=\frac{L_w(\lambda)}{E_d(\lambda,0^+)} \tag{2}$$

where $L_w(\lambda)$ is the spectral water-leaving radiance, and $E_d(\lambda,0^+)$ is the spectral downwelling irradiance just above the surface, calculated from their corresponding below-surface values using the approximations: $E_d(\lambda,0^+)=1.04\cdot E_d(\lambda,0^-)$ and $L_w(\lambda)=0.54\cdot L_u(\lambda,0^-)$ [*Austin*, 1974]. Here, $E_d(\lambda,0^-)$ was calculated as the exponential of the intercept ($z = 0$) of the least-square fit of the pooled profiles of ln [$E_d(\lambda, z)$] against depth z. Similarly, $L_u(\lambda,0^-)$ was calculated as the exponential of the intercept ($z = 0$) of the least-square fit of the pooled ln [$L_u(\lambda, z)$] profiles against depth z. In this study, only the $Rrs(\lambda, 0^+)$ derived at $\lambda = 443$, 488, 555, 667, and 678 nm (*Aqua*-MODIS wave bands) are used.

Table 2. Environmental Conditions During the Five GulfCarbon Cruises to the Northern Gulf of Mexico

		Salinity[a]	Water Temperature (°C)		
Season	Sampling Periods	Min-Max/Median	Min-Max/Median	Dominant Winds	Mean M-ARS Water Discharge[b] ($km^3\ d^{-1}$)
Winter 2009	9–18 Jan 2009	0–36.45/35.15	8.0–23.7/19.1	S-SW reversing to N-NE	1.85 (1.25)
Spring 2009	20–30 Apr 2009	0–36.95/34.20	15.1–24.6/22.7	SE	2.78 (2.49)
Summer 2009	19–29 Jul 2009	0–36.77/32.32	27.5–30.8/29.7	S-SW	1.41 (2.20)
Fall 2009	29 Oct to 7 Nov 2009	0–36.63/32.70	16.7–27.4/23.7	S-SE reversing to N-NE	2.82 (1.94)
Winter/spring 2010	11−20 Mar. 2010	0–36.48/28.32	10.6–20.3/17.0	NW	2.08 (2.68)

[a]Salinity/Water temperature ranges and median values correspond to the sampling grid of the CDOM samples (see Figure 1a).
[b]The number in parenthesis is the average M-ARS water discharge ($km^3\ d^{-1}$) during the 15 day period preceding the sampling period.

2.6. Daily Terrigenous DOC Flux From the Mississippi-Atchafalaya River System

Water discharge data from the U.S. Army Corps of Engineers (USACE) and DOC concentrations from the USGS National Stream Quality Accounting Network (NASQAN) were used to calculate terrigenous DOC fluxes from the Mississippi and Atchafalaya rivers between 1 July 2002 and 18 March 2013. Daily water discharge for the Mississippi River and Atchafalaya River is monitored at Tarbert Landing, MS, and Simmesport, LA, respectively, and was obtained from the USACE website (http://www.mvn.usace.army.mil/eng/edhd/wcontrol/discharge.asp). Concentrations of DOC are measured every 2 weeks in the Mississippi River near Melville, LA and the Atchafalaya River near St. Francisville, LA, and these data were obtained courtesy of the United States Geological Survey from the NASQAN website (http://water.usgs.gov/nasqan/). A linear interpolation was used to estimate daily DOC concentrations, and daily tDOC fluxes in the rivers were calculated as the product of the daily DOC concentration and daily water discharge. Daily tDOC flux anomalies were calculated by dividing daily tDOC fluxes by the long-term average tDOC flux between 1 July 2002 and 18 March 2013. Note the water discharge and tDOC flux of the M-ARS were considered here because runoff from both rivers can be exported across the region investigated in this study [*Zhang et al*., 2012b]. Furthermore, the water discharge and tDOC flux from the M-ARS were highly linearly correlated ($r = 0.997$ for water discharge, $r = 0.992$ for tDOC flux) to those of the Mississippi River between July 2002 and June 2013.

2.7. Terrigenous DOC Concentrations

The terrigenous DOC concentration, [tDOC], in water samples was determined as in equation (3)

$$[\mathrm{tDOC}] = [\mathrm{DOC}] \cdot f_{\mathrm{tDOC}} \tag{3}$$

where [DOC] is the measured DOC concentration, and f_{tDOC} is the fraction of terrigenous DOC in the sample estimated using equation (4)

$$f_{\mathrm{tDOC}} = \frac{\mathrm{TDLP}_9\text{-C}}{\mathrm{TDLP}_9\text{-C}_{\mathrm{M\text{-}ARS}}} \tag{4}$$

where TDLP_9-C is the DOC-normalized lignin yield in the sample, and $\mathrm{TDLP}_9\text{-C}_{\mathrm{M\text{-}ARS}}$ is a representative value of the DOC-normalized lignin yield of Mississippi-Atchafalaya river system water discharged to the study region. The $\mathrm{TDLP}_9\text{-C}_{\mathrm{M\text{-}ARS}}$ value was calculated for each cruise as in C. G. Fichot and R. Benner (submitted manuscript, 2014). Briefly, a strong linear relationship ($R^2 = 0.82$, $p = 0.0003$) exists in the Mississippi River and Atchafalaya River between total dissolved lignin phenol concentrations (TDLP_9, μmol C L^{-1}) and DOC concentrations (= tDOC in rivers). Daily TDLP_9 fluxes were derived from the daily Mississippi River and Atchafalaya River tDOC fluxes calculated in section 2.5.. For each cruise, $\mathrm{TDLP}_9\text{-C}_{\mathrm{M\text{-}ARS}}$ was calculated as the ratio of the TDLP_9 flux (mol C units) to M-ARS DOC flux over the time required to accumulate the freshwater volume present on the shelf at the time of the cruise (e.g., freshwater filling time). Filling time was used to approximate the residence time of freshwater in shelf surface waters [*Dinnel and Wiseman*, 1986], such that $\mathrm{TDLP}_9\text{-C}_{\mathrm{M\text{-}ARS}}$ is representative of the original riverine material that has been dispersed in the study area. Freshwater filling time was calculated using measured salinity, M-ARS water discharge, and shelf-wide precipitation and evaporation data. Freshwater filling times ranged from 2 to 3 months depending on the cruise (see C. G. Fichot and R. Benner, submitted manuscript, 2014 for details). The $\mathrm{TDLP}_9\text{-C}_{\mathrm{M\text{-}ARS}}$ (%DOC) values determined for each cruise were 0.396 (Winter 2009), 0.458 (Spring 2009), 0.489 (Summer 2009), 0.430 (Fall 2009), and 0.388 (Winter/spring 2010).

In this study, tDOC concentrations in marine waters were determined in two different ways, depending on whether the TDLP_9-C in the sample was directly measured (measured [tDOC]) or derived from the CDOM spectral slope coefficient (derived [tDOC]). For the measured [tDOC] ($n = 104$), TDLP_9-C in each sample was calculated from the measured DOC concentrations and measured concentrations of the nine dissolved lignin-derived phenols (TDLP_9). For the derived [tDOC] ($n = 222$), the TDLP_9-C in each sample was derived from $S_{275-295}$ as in *Fichot and Benner* [2012], using equation (5)

$$\text{TDLP}_9\text{-C} = \exp(\alpha + \beta \cdot S_{275-295}) + \exp(\gamma \cdot S_{275-295}) + \delta \cdot \exp(S_{275-295}) \quad (5)$$

where $\alpha = 3.172$, $\beta = -267.566$, $\gamma = 0.228$, and $\delta = -0.953$ are the parameters derived in *Fichot and Benner* [2012] for the northern Gulf of Mexico.

2.8. *Aqua*-MODIS Remote-Sensing Reflectances

Aqua-MODIS remote-sensing reflectance data, $Rrs(\lambda, 0^+)$ ($\lambda = 443$, 488, 555, 667, and 678 nm) were obtained from the NASA ocean color website (http://oceancolor.gsfc.nasa.gov). Data were subset over the northern Gulf of Mexico area and used in two different applications. Daily, 4 km resolution, L3b $Rrs(\lambda, 0^+)$ were binned over the 10–11 day duration of each research cruise (Table 1) and used for an end-to-end validation of the $S_{275-295}$-algorithm implementation with *Aqua*-MODIS (section 3.1.). In addition, monthly binned, 4 km resolution, L3m $Rrs(\lambda, 0^+)$ were used to implement the tDOC-algorithm for an 11 year time series analysis of remotely sensed, surface tDOC concentrations in the northern Gulf of Mexico between July 2002 and June 2013 (sections 3.2. and 3.3.). The daily $Rrs(\lambda, 0^+)$ binned over the 10–11 day duration of each research cruise provided the most appropriate data sets for direct comparison with in situ $S_{275-295}$ measurements, whereas the monthly binned $Rrs(\lambda, 0^+)$ provided a more homogenous coverage of the study region (spatially and temporally) and were therefore more suitable for a time series study.

2.9. Sea Surface Heights and Absolute Geostrophic Velocities

Sea surface heights above geoid and corresponding absolute geostrophic velocities over the northern Gulf of Mexico were obtained from the Aviso (Archiving, Validation and Interpretation of Satellite Oceanographic data) website (http://www.aviso.oceanobs.com/en/data/products/sea-surface-height-products/global.html). The weekly, Ssalto/*Duacs* Delayed-Time Maps of Absolute Dynamic Topography and absolute geostrophic velocities of the Reference series (DT-MADT "Ref") were used in this study. These homogenous data sets are based on two satellites (*Jason*−2/Envisat or *Jason*−1/Envisat, and *Topex/Poseidon/ERS*) and are available globally at a resolution of $1/3^\circ \times 1/3^\circ$.

2.10. Wind Vectors

Monthly mean, surface-level NCEP/NCAR Reanalysis wind vectors over the northern Gulf of Mexico between July 2002 and June 2013 were obtained from the NOAA Earth System Research Laboratory website (http://www.esrl.noaa.gov/psd/data/gridded/data.ncep.reanalysis.derived.surface.html). These wind vectors are available globally at a resolution of $2.5^\circ \times 2.5^\circ$ and were used for the time series analysis in this study. In addition, pentad (5 day) cross-calibrated multiplatform ocean surface wind vector L3.5A were obtained from the NASA Jet Propulsion Laboratory Physical Oceanography Distributed Active Archive Center (PO.DAAC) website (http://podaac.jpl.nasa.gov/dataset/CCMP_MEASURES_ATLAS_L4_OW_L3_5A_5DAY_WIND_VECTORS_FLK), and were used to evaluate the dominant wind conditions during each cruise.

3. Results and Discussion

3.1. $S_{275-295}$-Algorithm: Development, Validation, and Applicability

The 75 in situ $R_{rs}(\lambda)$ spectra and corresponding in situ $S_{275-295}$ collected during this study (Figure 1 and Table 1) facilitated the development of a simple but reliable empirical algorithm for the retrieval of $S_{275-295}$ from ocean color (multispectral $R_{rs}(\lambda)$). A multiple linear regression of ln ($S_{275-295}$) on the log-linearized $R_{rs}(\lambda)$ at $\lambda = 443$, 488, 555, 667, and 678 nm (equation (6)) was used to establish a strong empirical relationship between ocean color and $S_{275-295}$ in the northern Gulf of Mexico:

$$\begin{aligned} \ln(S_{275-295}) = \alpha + \beta \cdot \ln(Rrs(443)) + \gamma \cdot \ln(Rrs(488)) \\ + \delta \cdot \ln(Rrs(555)) + \varepsilon \cdot \ln(Rrs(667)) + \xi \cdot \ln(Rrs(678)) \end{aligned} \quad (6)$$

where $\alpha = -3.1221$, $\beta = 0.0673$, $\gamma = 0.3266$, $\delta = -0.07457$, $\varepsilon = -0.4599$, and $\xi = 0.2917$ are the derived regression coefficients. The $R_{rs}(\lambda)$ wave bands used here as predictors of $S_{275-295}$ were chosen as to match those of the *Aqua*-MODIS sensor and to optimize the accuracy of $S_{275-295}$ retrievals while minimizing the number of predictors. The $Rrs(\lambda)$ at $\lambda = 412$ nm was specifically discarded as a predictor variable for two reasons: (1) the inclusion of $Rrs(412)$ in the multiple linear regression did not significantly improve the accuracy of retrieved $S_{275-295}$ and (2) large errors are generally associated with satellite measurements of $Rrs(412)$ in

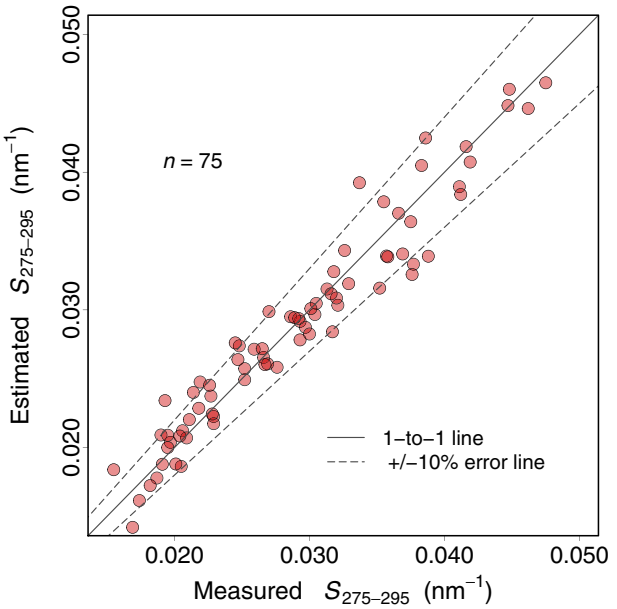

Figure 2. Estimated $S_{275–295}$ versus measured $S_{275–295}$ in a performance evaluation of the $S_{275–295}$ algorithm. Estimated $S_{275–295}$ are calculated from in situ measurements of multispectral $Rrs(\lambda, 0^+)$ $\lambda = 443$, 488, 555, 667, and 678 nm) using equation (6) and the corresponding multiple linear regression parameters. On average, $S_{275–295}$ can be estimated within <5% of the $S_{275–295}$ values measured in situ.

optically complex waters [*Sathyendranath*, 2000], such as those commonly found in the northern Gulf of Mexico. Performance evaluations of this $S_{275–295}$-algorithm (Figure 2) indicated $S_{275–295}$ can be estimated with an average uncertainty of ±5% from in situ $Rrs(\lambda)$ measurements. This uncertainty is relatively constant (homoskedastic) across the range of $S_{275–295}$ values encountered in the northern Gulf of Mexico (e.g., 0.015–0.050).

Implementation of the $S_{275–295}$-algorithm with *Aqua*-MODIS ocean color realistically reproduced the contrasting surface distributions of in situ $S_{275–295}$ observed during each cruise (Figure 3). A direct comparison between remotely sensed $S_{275–295}$ (referred to here as *Aqua*-MODIS $S_{275–295}$) and matching in situ $S_{275–295}$ from all cruises ($n = 206$) demonstrated that the implementation yields accurate $S_{275–295}$ retrievals over the entire range of $S_{275–295}$ values, even in the optically complex nearshore waters of the northern Gulf of Mexico (Figure 3a). On average, the *Aqua*-MODIS $S_{275–295}$ values were within 10% of the in situ $S_{275–295}$ values. The in situ $S_{275–295}$ values originally used in the development of the algorithm ($n = 75$) were also included in this validation (crossed-over-circle symbols in Figure 3). However, they were distinguished from the in situ $S_{275–295}$ that are independent from the algorithm development (regular-circle symbols in Figure 3), and did not significantly alter the estimated uncertainty associated with *Aqua*-MODIS $S_{275–295}$ (±9.0% versus ±9.5% on average).

The 10% uncertainty associated with *Aqua*-MODIS $S_{275–295}$ was larger than the ±5% uncertainty associated with $S_{275–295}$ values derived from in situ $Rrs(\lambda)$ measurements. Two main reasons can be responsible for this difference. Significant uncertainties can be associated with satellite measurements of $Rrs(\lambda)$ as a result of atmospheric interference, especially in the blue visible wave bands (e.g., $\lambda < 450$ nm) and in coastal areas [*Sathyendranath*, 2000]. In addition, the *Aqua*-MODIS $Rrs(\lambda)$ used in the validation were binned and averaged over the 10–11 day time period of each cruise. The remotely sensed $S_{275–295}$ presented in Figure 3 are therefore representative averages for each cruise time period, and were therefore not exactly matched in time with the in situ $S_{275–295}$ measurements. Time mismatch of up to a few days can therefore occur between remotely sensed and in situ $S_{275–295}$, thereby contributing to the 10% uncertainty estimated for *Aqua*-MODIS $S_{275–295}$. A more realistic uncertainty associated with *Aqua*-MODIS $S_{275–295}$ should therefore fall between ±5% and ±10%.

Current evidence suggests the synoptic, surface water monitoring of $S_{275–295}$ should be amenable to ocean-color remote sensing in most river-influenced marine systems. The present study and the recent work of *Fichot et al.* [2013] have demonstrated that empirical relationships between $S_{275–295}$ and ocean color can be established in the northern Gulf of Mexico and in the Arctic Ocean, respectively, two optically complex regions influenced by continental runoff. Gradients of ocean color in river-influenced marine systems are primarily controlled by continental runoff distributions because rivers are major sources of the most optically active seawater constituents (e.g., CDOM, phytoplankton, and suspended sediment) and of nutrients that fuel primary production. Furthermore, $S_{275–295}$ is a known tracer of tDOC in river-influenced ocean margins, and is therefore tightly linked to continental runoff distributions [*Fichot and Benner*, 2012; *Fichot et al.*, 2013]. Empirical relationships between $S_{275–295}$ (inherent optical property in the UV-B region) and ocean

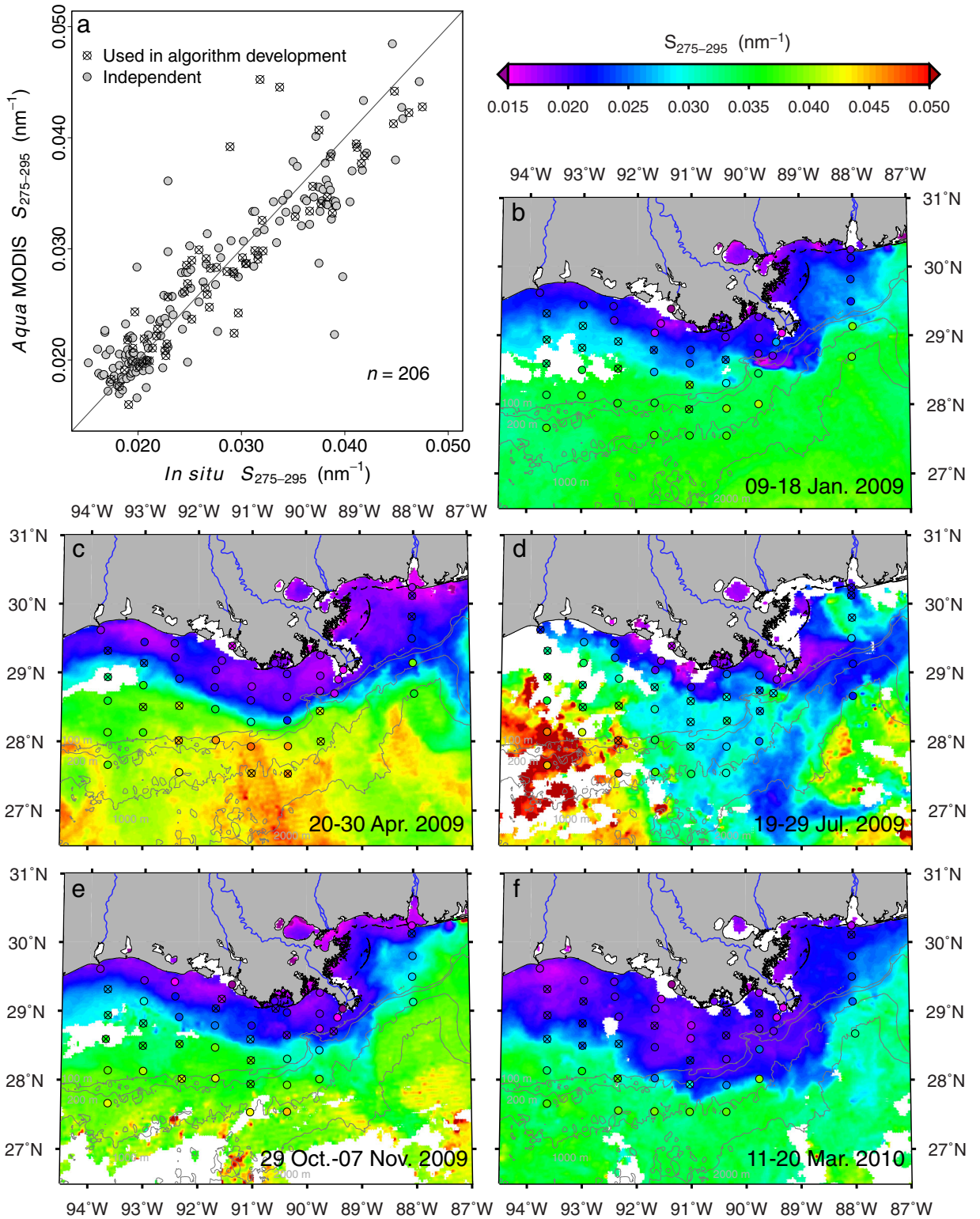

Figure 3. End-to-end validation of the $S_{275-295}$-algorithm implementation with *Aqua*-MODIS ocean color. Surface $S_{275-295}$ values measured in situ during all five cruises are directly compared to the $S_{275-295}$ values derived by implementing the $S_{275-295}$-algorithm on *Aqua*-MODIS ocean color (daily L3b $Rrs(\lambda)$ at 4 km resolution) binned over the 10–11 day time period corresponding to each cruise. The data used in the $S_{275-295}$-algorithm development were also included in this validation and are shown as crossed-over circles in all plots. (a) Scatterplot of *Aqua*-MODIS $S_{275-295}$ versus matched-up in situ $S_{275-295}$ from all cruises ($n = 206$). (b–f) Cruise-specific comparison between in situ $S_{275-295}$ and *Aqua*-MODIS $S_{275-295}$. The color within the circles correspond to the in situ $S_{275-295}$ values.

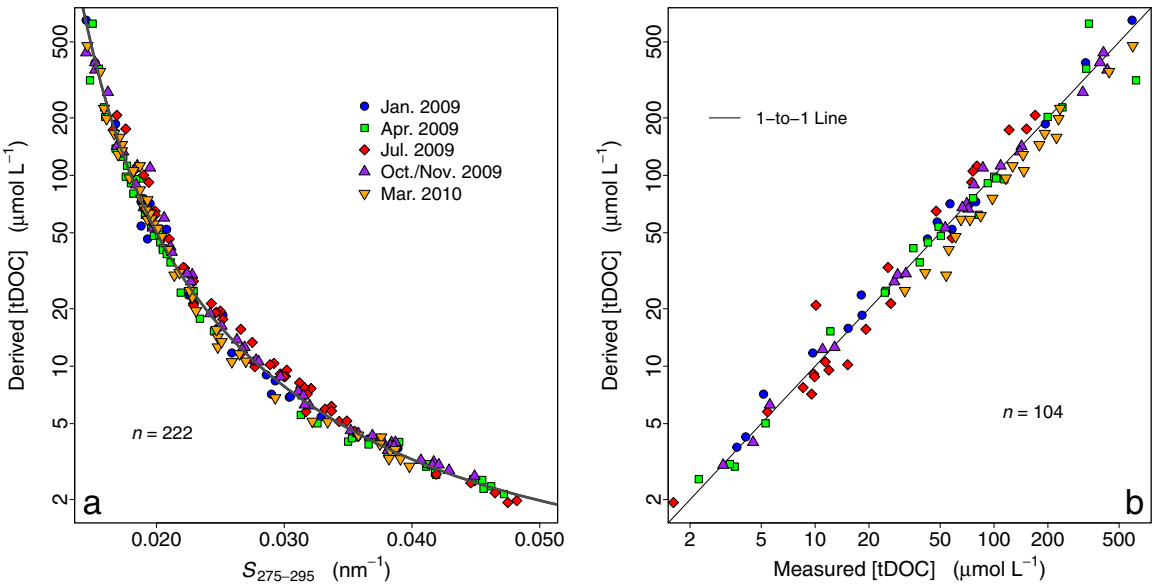

Figure 4. (a) Relationship between measured $S_{275-295}$ values and derived tDOC concentrations. The dark gray curve corresponds to the nonlinear regression of the derived tDOC concentration on the $S_{275-295}$ values using equation (7). Nonlinear equation (7) and its corresponding regression parameters can be used to calculate surface tDOC concentrations from remotely sensed $S_{275-295}$. (b) Derived tDOC concentrations versus measured tDOC concentrations. The measured tDOC concentrations are calculated using measured DOC concentrations and measured C-normalized lignin yields ($TDLP_9$-C). The derived tDOC concentrations are calculated using measured DOC concentrations and using C-normalized lignin yields ($TDLP_9$-C) derived from measured $S_{275-295}$ as in *Fichot and Benner* [2012].

color (apparent optical property in the visible region) can therefore be expected in these environments because continental runoff drives most of the variability of both ocean color and $S_{275-295}$. The empirical $S_{275-295}$-algorithm presented in this study (equation (6)) is similar in concept to the one developed for the Arctic Ocean [*Fichot et al.*, 2013], but was parameterized specifically for the northern Gulf of Mexico. Although region-specific parameterization is always desirable, its application to the Arctic Ocean data set [*Fichot et al.*, 2013; *Hooker et al.*, 2013] yielded reasonably accurate $S_{275-295}$ estimates (within ±10% error). Although this $S_{275-295}$-algorithm should perform reasonably in other river-influenced ocean margins, it is unlikely to perform well in marine environments where continental runoff contributions are small and variations in ocean color and $S_{275-295}$ are dominated by other processes (e.g., upwelling regions, open ocean).

3.2. Remote Sensing of Surface tDOC Concentrations in the Northern Gulf of Mexico

The $S_{275-295}$ represents an excellent proxy for terrigenous DOC concentrations in the northern Gulf of Mexico (Figure 4). Recently, the $S_{275-295}$ has been applied successfully as an optical proxy for the C-normalized yield of dissolved lignin ($TDLP_9$-C) and the fraction of terrigenous DOC in the surface waters of the northern Gulf of Mexico [*Fichot and Benner*, 2012] and Arctic Ocean [*Fichot et al.*, 2013]. In this study, the applicability of $S_{275-295}$ as a proxy was extended to the derivation of tDOC concentrations ([tDOC]). The nonlinear regression shown in equation (7) was used to parameterize a strong relationship between the $S_{275-295}$ values and tDOC concentrations of all 222 discrete samples collected during this study (Figure 4a):

$$\ln([\mathrm{tDOC}]) = \exp(\alpha - \beta \cdot S_{275-295}) + \exp(\gamma - \delta \cdot S_{275-295}) \quad (7)$$

where $\alpha = 4.2517$, $\beta = 255.6555$, $\gamma = 2.3415$, and $\delta = 54.4942$ are the derived parameters, and the nonlinear regression was weighted with a 1/[tDOC] function for a balanced fit across the large range of tDOC concentrations. Using equation (7), [tDOC] can be estimated with a ±10% uncertainty from accurate measurements of $S_{275-295}$.

The tDOC concentrations used in the nonlinear regression of equation (7) are "derived [tDOC]." In this study, derived [tDOC] differs from measured [tDOC] in that the $TDLP_9$-C used in their quantification was not directly measured, but derived from $S_{275-295}$ (see section 2.6. for details). Derived [tDOC] were used in the regression because a greater number of data were available, which allows for a better-constrained fit.

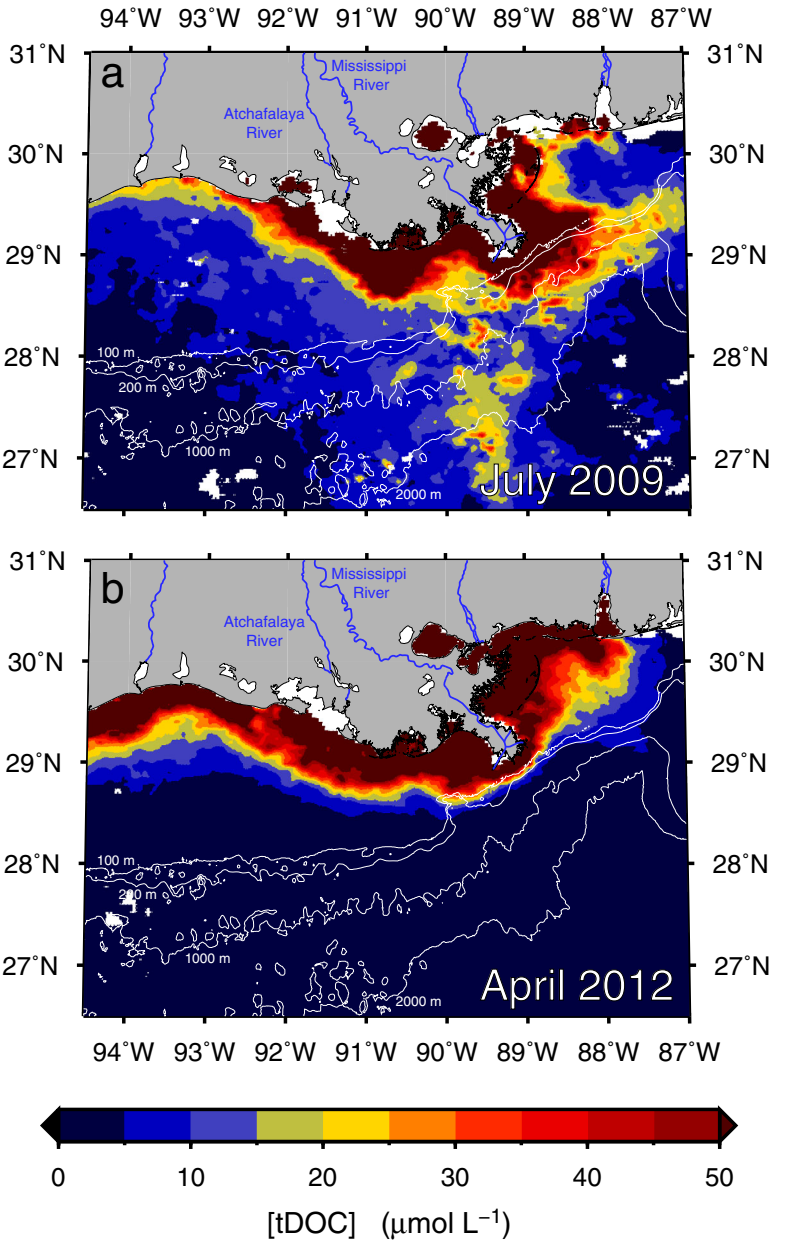

Figure 5. Implementation of the tDOC-algorithm in the northern Gulf of Mexico with *Aqua*-MODIS ocean color (monthly binned, L3m *Rrs*(λ) at 4 km resolution). (a) Remotely sensed, surface tDOC concentration in July 2009 during an important cross-shelf export event. (b) Remotely sensed, surface tDOC concentration in April 2012 at a time of low cross-shelf export.

However, $S_{275-295}$ is a robust proxy for $TDLP_9$-C [*Fichot and Benner*, 2012], and derived [tDOC] closely approximate measured [tDOC] ($\pm$16%) in this environment (Figure 4b). Using measured [tDOC] ($n = 104$) as the dependent variable in equation (7) produced an exponential curve almost identical to that in Figure 4a with the following regression parameters: $\alpha = 4.9191$, $\beta = 303.2523$, $\gamma = 2.4042$, and $\delta = 56.7117$.

The combined application of the $S_{275-295}$-algorithm (equation (6)) and tDOC proxy (equation (7)) facilitates the remote sensing of tDOC concentrations in surface waters of the northern Gulf of Mexico. For simplicity, this combined application is referred to as the "tDOC-algorithm" in the rest of this manuscript. Simple implementation of the tDOC-algorithm using *Aqua*-MODIS ocean color produced realistic distributions of tDOC concentrations in the northern Gulf of Mexico (Figure 5). An uncertainty analysis propagating the different sources of uncorrelated uncertainty in the tDOC-algorithm (see Appendix A) indicates the tDOC concentrations derived using *Aqua*-MODIS ocean color should be within $\pm$20–50% of the tDOC concentrations

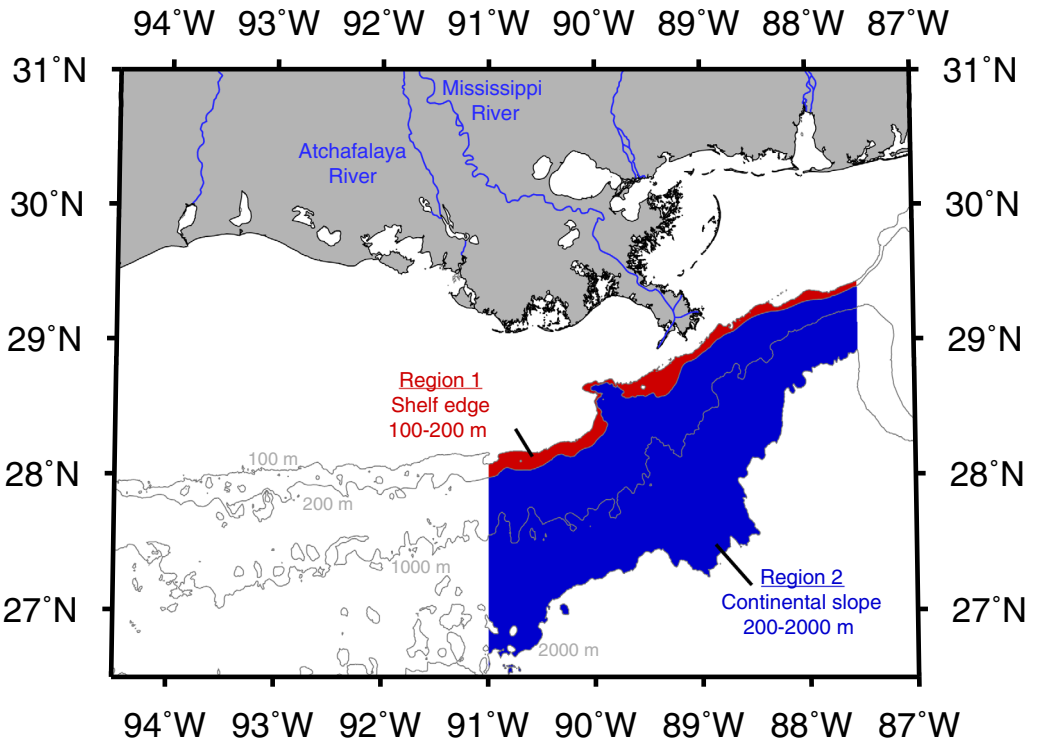

Figure 6. Regions of the northern Gulf of Mexico investigated in the time series analysis of surface tDOC concentrations (see Figures 7 and 8a). Region 1 is bound by the 100 and 200 m isobaths and represents the shelf edge. Region 2 is bound by the 200 and 2000 m isobaths represents the continental slope. Most of the river water export from the Mississippi-Atchafalaya river system occurs within this region [*Morey et al.*, 2003; *Schiller et al.*, 2011; *Zhang et al.*, 2012b].

measured in situ. This % uncertainty was dependent on the value of $S_{275-295}$, decreasing monotonically from ~50% at $S_{275-295} = 0.015$ nm^{-1} to ~20% at $S_{275-295} = 0.050$ nm^{-1}. This varying uncertainty along the $S_{275-295}$ continuum results primarily from the exponential dependence of ln([tDOC]) on $S_{275-295}$ in equation (7), which implies that the same ±7.5% uncertainty in $S_{275-295}$ results in a greater uncertainty in [tDOC] when $S_{275-295} = 0.015$ nm^{-1} than when $S_{275-295} = 0.050$ nm^{-1}.

3.3. Pulsed Cross-Shelf Export of tDOC Between 2002 and 2013

The tDOC-algorithm was applied to monthly binned *Aqua*-MODIS ocean color to trace tDOC transported from the Mississippi-Atchafalaya River System (M-ARS) across the shelf boundary (200 m isobath) and onto the oceanic waters of the northern Gulf of Mexico over the past 11 years. Surface tDOC concentrations were remotely sensed over the shelf edge (100–200 m isobaths, Region 1) and continental slope (200–2000 m isobaths, Region 2) of a region of the northern Gulf of Mexico bound by the 87.5°W and 91°W meridians (Figure 6). This specific region was chosen because much of the cross-shelf export of M-ARS freshwater occurs within this longitudinal window [*Morey et al.*, 2003; *Schiller et al.*, 2011; *Zhang et al.*, 2012b]. Furthermore, the close proximity of the Mississippi River mouth to the shelf edge in that region indicates recently discharged continental runoff, including terrigenous organic matter and nutrients, can be rapidly exported to the continental slope and potentially enhance biological production and respiration in these relatively oligotrophic waters.

Remote sensing of surface tDOC concentrations over the continental slope (Region 2) indicated much of the cross-shelf export of tDOC occurred during a few sporadic events between July 2002 and June 2013 (Figures 7 and 8a). Surface water tDOC concentrations during these events increased tenfold from background values of 2–4 μmol L^{-1} to 30–35 μmol L^{-1} over much of the continental slope (Figure 7). The average surface water tDOC concentration for the whole continental slope region (Region 2) increased from a background of ~3 μmol L^{-1} to almost 20 μmol L^{-1} (Figure 8a). Large pulses of tDOC on the continental slope did not occur every year, thereby indicating a large interannual variability in the cross-shelf export of tDOC in this region. The continental slope was little influenced by tDOC from the M-ARS during 2005–2007

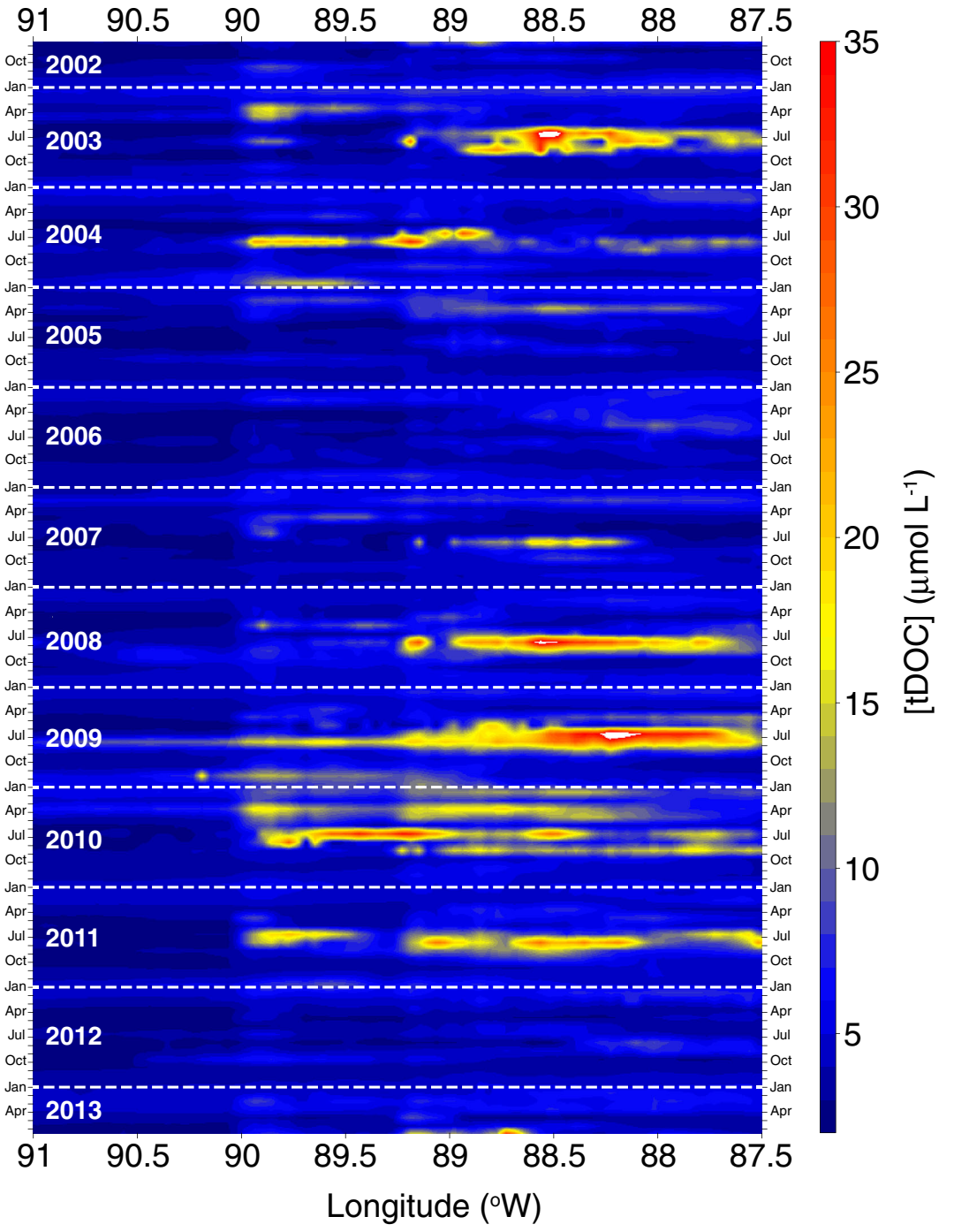

Figure 7. Time series of average tDOC concentrations versus longitude (Hovmöller diagram) on the continental slope (200–2000 m, Region 2 in Figure 6). For any given month (*y* axis) and longitude (*x* axis) on this plot, the corresponding [tDOC] is an average over the latitude range of the continental slope at that longitude and for that month.

and 2012, with minimal tDOC concentrations observed in 2006 and 2012. In contrast, several major pulses of M-ARS tDOC to the continental slope were observed during 2003–2004 and 2008–2011, with maximal tDOC concentrations observed in 2009 and 2010 (Figure 8a).

The major cross-shelf export events observed between July 2002 and June 2013 typically occurred during summer, when wind-driven dynamics were favorable for the offshore transport of shelf surface water (Figures 7, 8a, and 8b). During fall, winter and spring, prevalent easterly and northeasterly winds typically drive

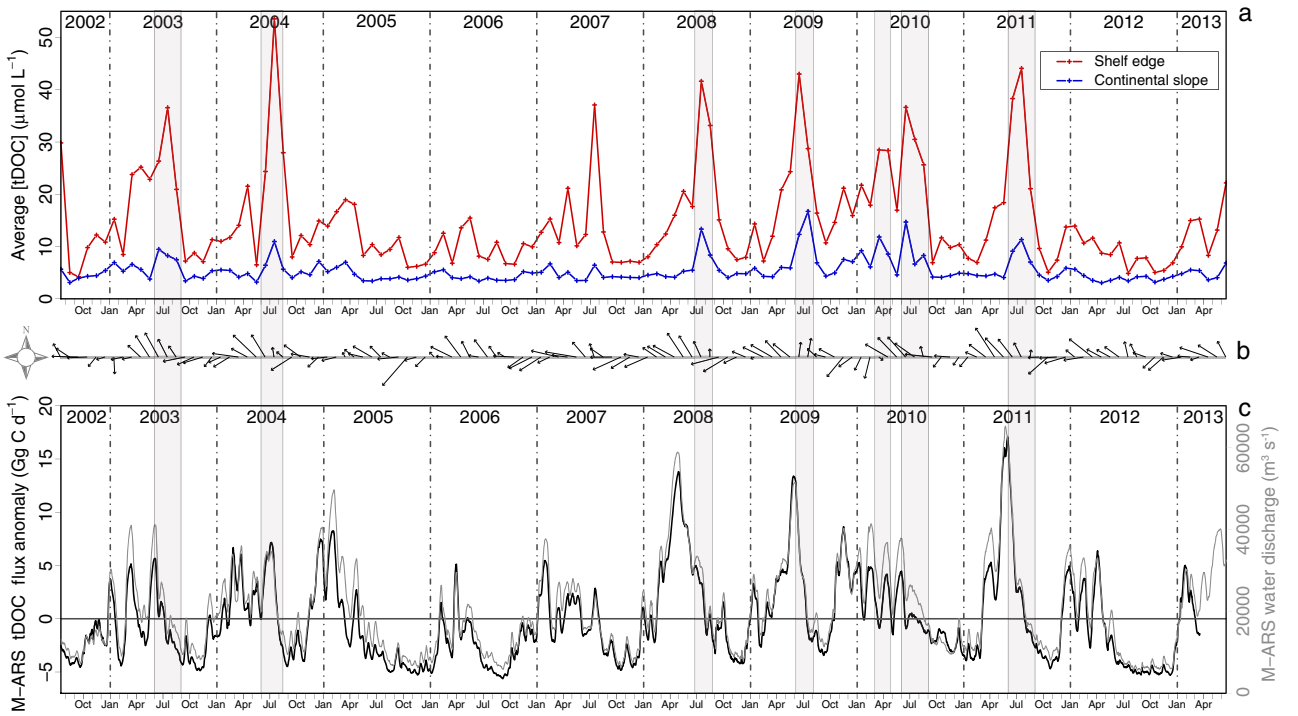

Figure 8. (a) Time series of average surface tDOC concentration on the shelf edge (100–200 m, Region 1 in Figure 6) and on the continental slope (200–2000 m, Region 2 in Figure 6) between July 2002 and June 2013. The seven most important cross-shelf export events are highlighted (shaded areas). (b) Time series of the monthly averaged wind velocity vector over the northern Gulf of Mexico region (see Figure 1) between July 2002 and June 2013. Southerly winds (upward arrows) are favorable for cross-shelf export in this region. (c) Time series of the tDOC flux anomaly (black line, left *y* axis) and water discharge (gray line, right *y* axis) from the Mississippi-Atchafalaya River System (M-ARS) between July 2002 and June 2013. The anomaly is relative to the average tDOC flux between 1 July 2002 and 18 March 2013. Important cross-shelf export events always occurred during periods of high water discharge (anomalously high tDOC flux) and favorable wind conditions.

westward currents on the shelf and promote alongshore transport of M-ARS water down the Louisiana-Texas coast [*Ohlmann and Niiler*, 2005]. These conditions minimize exchange with offshore surface waters. However, a shift to predominantly southeasterly and southerly winds during summer forces the Ekman transport of M-ARS water eastward toward the De Soto canyon, where it is rapidly transported to the continental slope and can interact with the mesoscale Loop-Current eddy field of the deep Gulf of Mexico [*Morey et al*., 2003]. Nevertheless, periods of favorable wind during summer did not always coincide with major cross-shelf export events. Low water discharge and anomalously low tDOC fluxes from the M-ARS during or preceding periods of favorable summer winds appeared responsible for the absence of major cross-shelf export events in 2005, 2006, 2007, and 2012 (Figures 8a and 8b).

Notable cross-shelf export events also occurred during other seasons, particularly during winter and spring (Figures 7 and 8a). The unseasonal, major offshore transport of tDOC in the spring of 2010 can be attributed to persistent northwesterly winds at a time of high discharge, as demonstrated in *Huang et al*. [2013] and in this study (Figure 8). Cold fronts can lead to short-term reversals of the prevalent easterly/northeasterly wind pattern and drive eastward Ekman transport and eddy entrainment [*Walker et al*., 2005], although recent evidence suggests these reversals are often too short to promote efficient export across the shelf [*Schiller et al*., 2011]. Finally, tropical storms and hurricanes during late summer and fall can also enhance cross-shelf export in this region [*Yuan et al*., 2004; *Stone et al*., 2005; *D'Sa et al*., 2011], but our observations suggest it does not always constitute an important mechanism of cross-shelf export. For example, the passage of Hurricane Lili (early October 2002) described in *Yuan et al*. [2004] was a noticeable event in our time series (Figure 7), but the passage of Hurricane Katrina in late August 2005 [*Gierach and Subrahmanyam*, 2008] had very little impact on the continental-slope tDOC concentrations, consistent with other observations that offshore bio-optical conditions were rapidly restored to that prior to the storm [*Lohrenz et al*., 2008].

The time series of remotely sensed tDOC concentrations revealed that major tDOC pulses in continental-slope surface waters were tightly linked to the water discharge and tDOC flux anomalies of the M-ARS

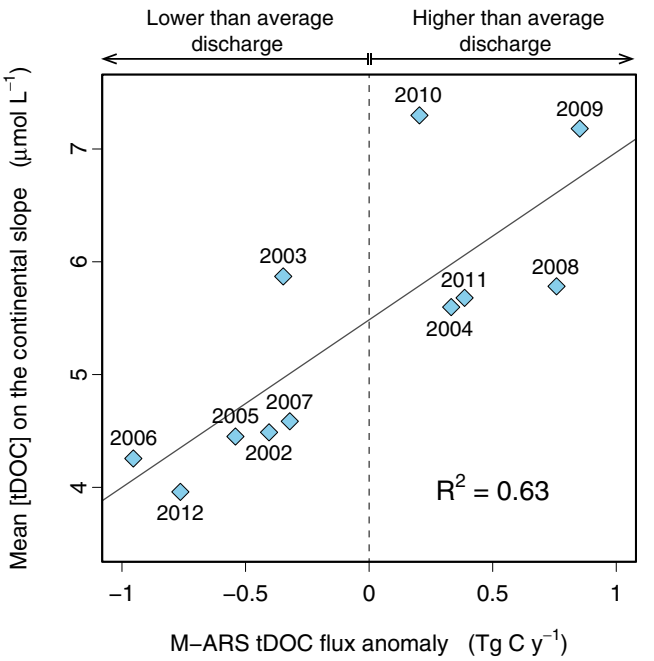

Figure 9. Mean surface tDOC concentration on the continental slope (200–2000 m, Region 2 in Figure 6) averaged during each year versus annual tDOC flux anomaly from the Mississippi-Atchafalaya River System (M-ARS).

(Figures 8 and. 9). Between July 2002 and June 2013, major tDOC pulses in continental-slope surface waters were always preceded by high river discharge and a prolonged positive anomaly in M-ARS tDOC fluxes (Figure 8). As mentioned earlier, favorable wind conditions alone did not trigger a major export of tDOC unless a large positive anomaly in M-ARS tDOC flux preceded the wind event. Variations in the tDOC fluxes are primarily driven by changes in water discharge in this river system (Figure 8b), and the area and shape of the Mississippi River plume depend strongly on the magnitude of the water discharge [*Walker et al*., 1996, 2005]. Higher than average river discharge can enhance cross-shelf export of tDOC by pushing the frontal location of the plume across the shelf toward the continental slope, thereby facilitating offshore entrainment by mesoscale eddy circulation in the deep Gulf of Mexico. On an annual basis, the M-ARS tDOC flux anomaly explained 63% of the variability ($R^2 = 0.63$, p = 0.003) in the average tDOC concentration of the continental slope region (Region 2), thereby indicating continental-slope surface waters are generally enriched with tDOC during years of high river discharge (Figure 9). Note a lag of −15 days was applied to the tDOC flux anomaly to maximize the R^2 against the continental-slope tDOC concentrations. This lag represents a reasonable average transport time between the river gauge and the continental slope, considering that water transit from river gauge to river mouth is ∼ 5–7 days in the Mississippi and Atchafalaya rivers [*Shen et al*., 2012], and an average transport time of ∼8–10 days from the river mouth to the continental slope is realistic [*Walker et al*., 1996; *Schiller et al*., 2011].

Mesoscale eddies produced by the Loop Current System enhanced cross-shelf export on several occasions between July 2002 and June 2013. Mesoscale eddies are known to impinge on the shelf break south of the Mississippi River delta [*Ohlmann et al*., 2001], often when favorable winds and high discharge facilitate the transport of river water on the continental slope. Under these circumstances, mesoscale eddies can efficiently entrain tDOC over the continental slope and offshore [*Morey et al*., 2003; *Walker et al*., 2005; *Schiller et al*., 2011], although the close proximity of eddies to the Mississippi River mouth alone can be a sufficient condition for the cross-shelf entrainment of tDOC even in the absence of favorable winds [*Schiller et al*., 2011]. This mechanism of eddy entrainment was clearly observed in the summer of 2003 and 2011, for instance, when large anticyclonic eddies shed from the Loop Current impinged on the shelf break and enhanced tDOC export east of the 89°W meridian (Figure 10). This mechanism has also been shown to occasionally entrain filaments of M-ARS water well beyond the continental slope and to the Loop Current, where it can become part of the Gulf Stream and eventually reach the North Atlantic Ocean [*Ortner et al*., 1995; *Gilbert et al*., 1996; *Hu et al*., 2005]. The impingement of a counter-rotating pair of eddies on the continental slope can be a particularly effective mechanism of cross-shelf export [*Stone et al*., 2005; *Walker et al*., 2005; *Schiller et al*., 2011]. From May to July 2009, a pair of counter-rotating mesoscale eddies impinged and evolved slowly on the shelf break during favorable wind conditions and high river discharge, and thereby enhanced cross-shelf export of tDOC west of the 89°W meridian (Figure 11). This eddy-pair mechanism contributed to the spectacular, shelf-wide export event of June-July 2009.

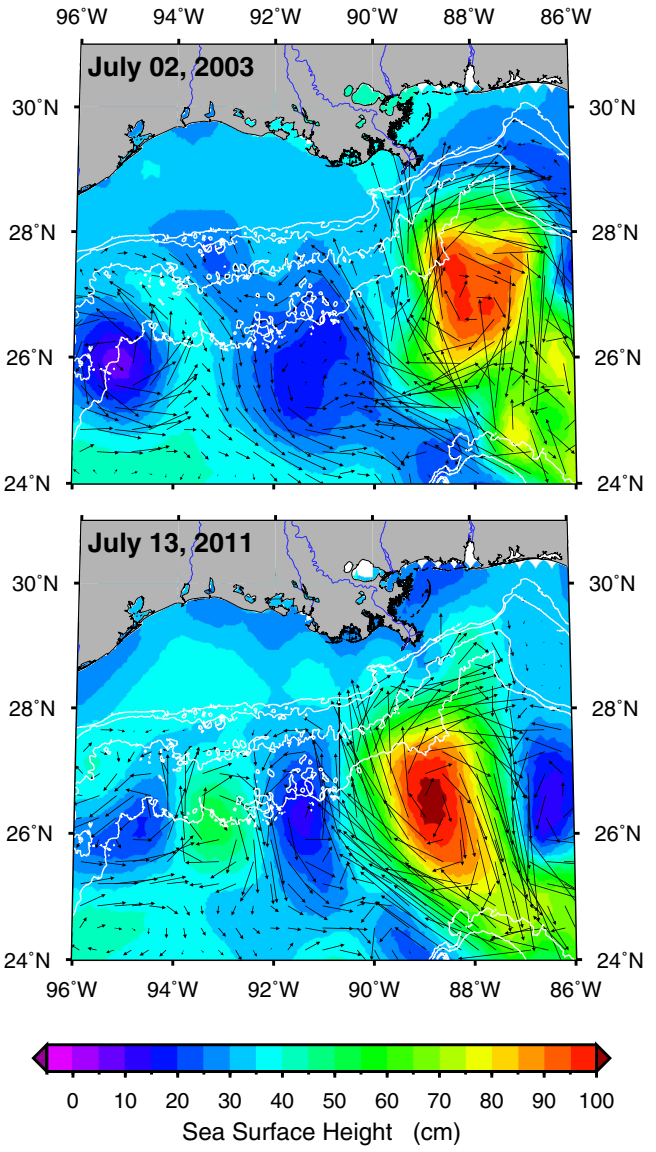

Figure 10. Sea surface heights and absolute geostrophic velocities (Aviso DT-MADT "Ref" product) over the northern Gulf of Mexico during Loop Current anticyclonic eddy intrusions on the continental slope in (a) July 2003 and (b) July 2011.

3.4. Implications of a Pulsed, Cross-Shelf Export of tDOC

The cross-shelf export of M-ARS tDOC and associated river-borne and shelf-derived materials can have a strong influence on biological community structure and function in Gulf of Mexico waters located beyond the continental shelf boundary. The tenfold increase in tDOC concentration (2–4 μmol L^{-1} to 30–35 μmol L^{-1}) observed periodically over much of the continental slope represents a ~50% addition to ambient DOC concentrations (60–70 μmol L^{-1}) typically observed in these surface waters [*Benner and Opsahl*, 2001; *Fichot and Benner*, 2011]. These pulses of tDOC and associated elements are important sources of organic matter and nutrients (e.g., N, P, Si, Fe) that can enhance primary production, which is often nutrient limited in these surface waters [*Dortch and Whitledge*, 1992; *Lohrenz et al.*, 1999; *Chen et al.*, 2000]. Riverine iron, in particular, could enhance nitrogen fixation by *Trichodesmium* spp. in the Gulf of Mexico [*Mulholland et al.*, 2006], where it has been shown to be Fe limited [*Lenes et al.*, 2001]. The exported tDOC includes a variety of chromophores [*Blough and Del Vecchio*, 2002; *Stubbins et al.*, 2010; *Fichot and Benner*, 2012] that also impact primary production by regulating the attenuation of ultraviolet and visible radiation in the water column. Photochemical transformations of terrigenous organic matter can stimulate bacterial growth and respiration and generate bioavailable forms of nutrients [*Kieber et al.*, 1989; *Mopper and Kieber*, 2002; *Xie et al.*, 2012]. Overall, these export events and impacts on biological processes can have complex effects on net air-sea CO_2 fluxes in Gulf of Mexico waters. Furthermore, cross-shelf export of M-ARS inputs inevitably leads to the transport of various pollutants (e.g., petroleum and xenobiotics) to sensitive marine ecosystems where they can be harmful to biota and bioaccumulate in the food web [*Torres et al.*, 2008]. Export across the shelf boundary to the Loop Current system and the Gulf Stream also represents a mechanism by which persistent pollutants and pathogens can be transported over long distances and dispersed over large scales.

The pulsed nature of tDOC concentrations on the continental slope suggests the cross-shelf export of tDOC and other materials will be sensitive to future changes in climate and human activities (e.g., land use). Over the past decade (2002–2013), the export of tDOC to surface waters of the continental slope was dominated by a few major but sporadic export events, and as a result exhibited considerable interannual variability.

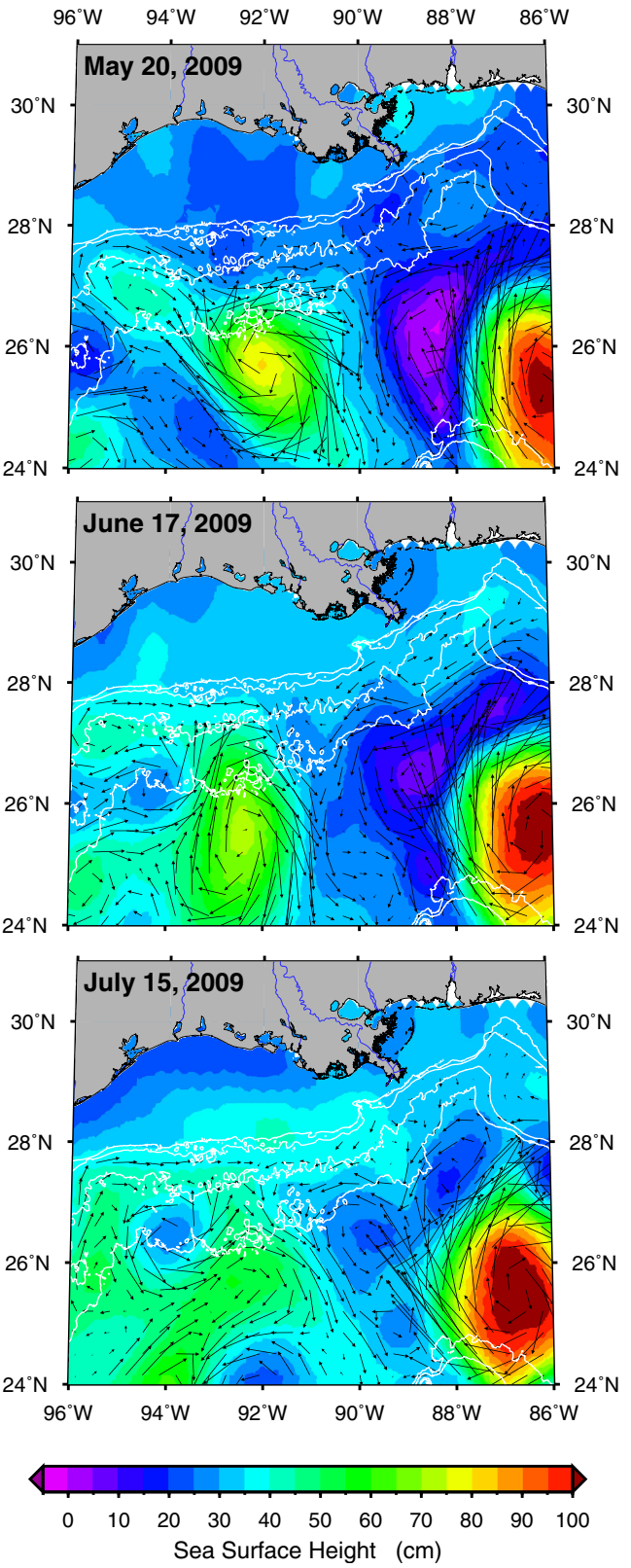

Figure 11. Sea surface heights and absolute geostrophic velocities (Aviso DT-MADT "Ref") over the northern Gulf of Mexico showing a counter-rotating pair of eddies impinging and slowly evolving on the continental slope between May and July 2009. In addition to high river discharge (anomalously high tDOC flux) and very favorable wind conditions, this eddy-pair mechanism enhanced the southward transport of tDOC and contributed to the spectacular cross-shelf export event of June-July 2009 (see Figure 5a).

This study clearly revealed these major tDOC export events were tightly linked to the occurrence of favorable wind conditions during or immediately following positive anomalies of the M-ARS tDOC flux (river discharge), with mesoscale eddies impinging on the shelf break occasionally enhancing cross-shelf export. Although the cooccurrence of these three factors provide the ideal setting for major export events, the magnitude of tDOC flux anomalies emerged as the main controlling factor of cross-shelf export on an annual basis. The recent trends in land use and hydroclimatic conditions over the Mississippi River basin [*Qian et al*., 2007; *Schilling et al*., 2010; *Groisman et al*., 2012] thus presage potential changes in river discharge that could affect the cross-shelf export of tDOC and its influence on the continental shelf and slope. Recent changes in the Loop Current's eddy shedding [*Vukovich*, 2012] could also alter the dynamics of the mesoscale eddy field and affect its capacity to entrain river plume water.

4. Conclusion

The tDOC-algorithm presented in this study provides a new capability for the real-time and long-term monitoring of surface tDOC concentrations in the northern Gulf of Mexico using ocean-color remote sensing. Implementations of this algorithm will allow direct assessment of future variations in the cross-shelf export of terrigenous material from the Mississippi-Atchafalaya River System, and help elucidate its potential linkages to climate- or human-induced changes. The algorithm should find applicability in biogeochemical models of the continental shelf [*Hofmann et al*., 2010], contribute to a better understanding of the complex, buoyancy-driven shelf circulation of the northern Gulf of Mexico by providing a reliable means to validate the results of high-resolution coastal models [*Schiller et al*., 2011; *Zhang et al*., 2012a], and integrate well with emerging approaches for the remote sensing of sea surface salinity in coastal regions [*Gierach et al*., 2013]. Despite its limitation as a tracer of terrigenous inputs, remotely sensed chlorophyll-a is typically used for the validation of coastal models. The tDOC-algorithm presented here has the advantage of being parameterized using the lignin biomarker, which substantiates the terrigenous origin of the remotely sensed signal.

Appendix A

An uncertainty analysis was carried out to calculate the uncertainty associated with the remotely sensed [tDOC], and included three sources of uncertainty (see section 3.1.).

1. a $\pm$ 7.5% uncertainty in remotely sensed $S_{275-295}$, relative to $S_{275-295}$ measured in situ.

2. a $\pm$ 10% uncertainty in "derived [tDOC]" estimated from $S_{275-295}$.

3. a $\pm$ 16% uncertainty in "measured [tDOC]" relative to the "derived [tDOC]."

As can be seen in Figures 2–4, these %-uncertainties were relatively constant along their respective range of values. The sources of uncertainty were also uncorrelated with each other.

The theoretical uncertainty was calculated at every 0.001 nm^{-1} increment in $S_{275-295}$ between 0.015 and 0.050 nm^{-1}. At each $S_{275-295}$ increment, a random %-error from a normal distribution of mean 7.5 was added to the value of $S_{275-295}$ in order to simulate the $\pm$7.5% uncertainty associated with remotely sensed $S_{275-295}$ (uncertainty 1). That slightly inaccurate $S_{275-295}$ value was then used in equation (7) to calculate a corresponding "derived [tDOC]" value, to which a random %-error from a normal distribution of mean 10 was also added to simulate the $\pm$10% uncertainty in "derived [tDOC]" estimated from $S_{275-295}$ (uncertainty 2). Finally, a random %-error from a normal distribution of mean 16 was added to that "derived [tDOC]" estimate in order to simulate the $\pm$16% uncertainty in "derived [tDOC]" relative to the "measured [tDOC]" (uncertainty 3). At each $S_{275-295}$ increment, the estimated [tDOC] was then compared to a reference [tDOC] calculated by assuming 0% error for all three sources of uncertainty, and the %-error was calculated. This operation was repeated a large number of times (>1,000,000), such that each $S_{275-295}$ increment was populated by a distribution of >1,000,000 %-error estimates. The median of the % error distribution was then determined at each $S_{275-295}$ increment and ranged from about 50% when $S_{275-295} = 0.015$ nm^{-1} to about 20% when $S_{275-295} = 0.050$ nm^{-1}.

Acknowledgments

We thank Wei-Jun Cai for providing a berth on the GulfCarbon cruises, and we are grateful to Leanne Powers, Kevin Martin, and the crews of the R/V *Cape Hatteras* and the R/V *Hugh Sharp* for their assistance with sample collection during the GulfCarbon cruises. We are grateful to the National Aeronautics and Space Administration for providing public access to the *Aqua*-MODIS data and the PO.DAAC pentad wind vectors data, to Aviso (Archiving, Validation and Interpretation of Satellite Oceanographic data) for providing access to the sea surface height and absolute geostrophic velocity data, and finally to the National Oceanographic and Atmospheric Administration for providing the NCEP/NCAR reanalysis wind vector data. Maps in this study were made using the Generic Mapping Tools (http://gmt.soest.hawaii.edu). We also thank Tanya Mildner, Alexander Yankovsky, and two anonymous reviewers for their insights. Funding for this work was provided by the National Science Foundation (NSF, grants 0850653 and 0713915 to Ronald Benner, 0752254 to Steven E. Lohrenz, and 0752110 to Wei-Jun Cai) and by the National Aeronautics and Space Administration (NASA, NNX10AU06G and NNX12AP84G to Steven E. Lohrenz).

References

Austin, R. (1974), The remote sensing of spectral radiance from below the ocean surface, in *Optical Aspects of Oceanography*, pp. 317–344, Academic Press, London, U. K.

Benner, R., and S. Opsahl (2001), Molecular indicators of the sources and transformations of dissolved organic matter in the Mississippi river plume, *Org. Geochem.*, *32*, 597–611.

Benner, R., and M. Strom (1993), A critical evaluation of the analytical blank associated with DOC measurements by high-temperature catalytic oxidation, *Mar. Chem.*, *41*(1-3), 153–160, doi:10.1016/0304-4203(93)90113-3.

Benner, R., P. Louchouarn, and R. M. W. Amon (2005), Terrigenous dissolved organic matter in the Arctic Ocean and its transport to surface and deep waters of the North Atlantic, *Global Biogeochem. Cycles*, *19*, GB2025, doi:10.1029/2004GB002398.

Bianchi, T. S. (2011), The role of terrestrially derived organic carbon in the coastal ocean: A changing paradigm and the priming effect, *Proc. Natl. Acad. Sci. U. S. A.*, *108*(49), 19,473–19,481, doi:10.1073/pnas.1017982108.

Blough, N. V., and R. Del Vecchio (2002), Chromophoric DOM in the coastal environment, in *Biogeochemistry of Marine Dissolved Organic Matter*, edited by D. A. Hansell and C. A. Carlson, pp. 509–546, Academic, San Diego, Calif.

Chen, X., S. E. Lohrenz, and D. A. Wiesenburg (2000), Distribution and controlling mechanisms of primary production on the Louisiana–Texas continental shelf, *J. Mar. Syst.*, *25*(2), 179–207, doi:10.1016/S0924-7963(00)00014-2.

D'Sa, E. J., R. L. Miller, and C. Del Castillo (2006), Bio-optical properties and ocean color algorithms for coastal waters influenced by the Mississippi River during a cold front, *Appl. Opt.*, *45*(28), 7410–7428.

D'Sa, E. J., M. Korobkin, and D. S. Ko (2011), Effects of Hurricane Ike on the Louisiana-Texas coast from satellite and model data, *Remote Sens. Lett.*, *2*(1), 11–19, doi:10.1080/01431161.2010.489057.

Del Castillo, C. E., and R. L. Miller (2008), On the use of ocean color remote sensing to measure the transport of dissolved organic carbon by the Mississippi River Plume, *Remote Sens. Environ.*, *112*(3), 836–844, doi:10.1016/j.rse.2007.06.015.

Dinnel, S. P., and W. J. Wiseman (1986), Fresh water on the Louisiana and Texas shelf, *Cont. Shelf Res.*, *6*, 765–784, doi:10.1016/0278-4343(86)90036-1.

Dittmar, T., and G. Kattner (2003), The biogeochemistry of the river and shelf ecosystem of the Arctic Ocean: A review, *Mar. Chem.*, *83*(3-4), 103–120, doi:10.1016/S0304–4203(03)00105-1.

Dittmar, T., K. Whitehead, E. C. Minor, and B. P. Koch (2007), Tracing terrigenous dissolved organic matter and its photochemical decay in the ocean by using liquid chromatography/mass spectrometry, *Mar. Chem.*, *107*(3), 378–387, doi:10.1016/j.marchem.2007.04.006.

Dortch, Q., and T. E. Whitledge (1992), Does nitrogen or silicon limit phytoplankton production in the Mississippi River plume and nearby regions?, *Cont. Shelf Res.*, *12*(11), 1293–1309.

Fichot, C. G., and R. Benner (2011), A novel method to estimate DOC concentrations from CDOM absorption coefficients in coastal waters, *Geophys. Res. Lett.*, *38*, L03610, doi:10.1029/2010GL046152.

Fichot, C. G., and R. Benner (2012), The spectral slope coefficient of chromophoric dissolved organic matter (S275–295) as a tracer of terrigenous dissolved organic carbon in river-influenced ocean margins, *Limnol. Oceanogr.*, *57*(5), 1453–1466, doi:10.4319/lo.2012.57.5.1453.

Fichot, C. G., K. Kaiser, S. Hooker, R. Amon, M. Babin, S. Bélanger, S. Walker, and R. Benner (2013), Pan-Arctic distributions of continental runoff in the Arctic Ocean, *Sci. Rep.*, *3*, 1053, doi:10.1038/srep01053.

Gierach, M. M., and B. Subrahmanyam (2008), Biophysical responses of the upper ocean to major Gulf of Mexico hurricanes in 2005, *J. Geophys. Res.*, *113*, C04029, doi:10.1029/2007JC004419.

Gierach, M. M., J. Vazquez-Cuervo, T. Lee, and V. M. Tsontos (2013), Aquarius and SMOS detect effects of an extreme Mississippi River flooding event in the Gulf of Mexico, *Geophys. Res. Lett.*, *40*, 5188–5193, doi:10.1002/grl.50995.

Gilbert, P. S., T. N. Lee, and G. P. Podesta (1996), Transport of anomalous low-salinity waters from the Mississippi River flood of 1993 to the Straits of Florida, *Cont. Shelf Res.*, *16*(8), 1065–1085, doi:10.1016/0278-4343(95)00056-9.

Groisman, P. Y., R. W. Knight, and T. R. Karl (2012), Changes in Intense Precipitation over the Central United States, *J. Hydrometeorol.*, *13*(1), 47–66, doi:10.1175/jhm-d-11–039.1.

Hedges, J. I., P. G. Hatcher, J. R. Ertel, and K. J. Meyers-Schulte (1992), A comparison of dissolved humic substances from seawater with Amazon River counterparts by 13C-NMR spectrometry, *Geochim. Cosmochim. Acta*, *56*(4), 1753–1757, doi:10.1016/0016-7037(92)90241-A.

Hedges, J. I., R. G. Keil, and R. Benner (1997), What happens to terrestrial organic matter in the ocean?, *Org. Geochem.*, *27*(5-6), 195–212, doi:10.1016/S0146-6380(97)00066-1.

Helms, J. R., A. Stubbins, J. D. Ritchie, E. C. Minor, D. J. Kieber, and K. Mopper (2008), Absorption spectral slopes and slope ratios as indicators of molecular weight, source, and photobleaching of chromophoric dissolved organic matter, *Limnol. Oceanogr.*, *53*(3), 955–969.

Hernes, P. J., and R. Benner (2002), Transport and diagenesis of dissolved and particulate terrigenous organic matter in the North Pacific Ocean, *Deep Sea Res., Part I*, *49*(12), 2119–2132.

Hofmann, E. E., et al. (2010), Modeling the dynamics of continental shelf carbon, *Annu. Rev. Mar. Sci.*, *3*(1), 93–122, doi:10.1146/annurev-marine-120709-142740.

Hoge, F. E., M. E. Williams, R. N. Swift, J. K. Yungel, and A. Vodacek (1995), Satellite retrieval of the absorption coefficient of chromophoric dissolved organic matter in continental margins, *J. Geophys. Res.*, *100*(C12), 24,847–24,854.

Hooker, S. B., J. H. Morrow, and A. Matsuoka (2013), Apparent optical properties of the Canadian Beaufort Sea—Part 2: The 1% and 1 cm perspective in deriving and validating AOP data products, *Biogeosciences*, *10*(7), 4511–4527, doi:10.5194/bg-10-4511-2013.

Hu, C., F. E. Muller-Karger, D. C. Biggs, K. L. Carder, B. Nababan, D. Nadeau, and J. Vanderbloemen (2003), Comparison of ship and satellite bio-optical measurements on the continental margin of the NE Gulf of Mexico, *Int. J. Remote Sens.*, *24*(13), 2597–2612, doi:10.1080/0143116031000067007.

Hu, C., J. R. Nelson, E. Johns, Z. Chen, R. H. Weisberg, and F. E. Müller-Karger (2005), Mississippi River water in the Florida Straits and in the Gulf Stream off Georgia in summer 2004, *Geophys. Res. Lett.*, *32*, L14606, doi:10.1029/2005GL022942.

Huang, W.-J., W.-J. Cai, R. M. Castelao, Y. Wang, and S. E. Lohrenz (2013), Effects of a wind-driven cross-shelf large river plume on biological production and CO2 uptake on the Gulf of Mexico during spring, *Limnol. Oceanogr.*, *58*(5), 1727–1735.

Johannessen, S. C., and W. L. Miller (2001), Quantum yield for the photochemical production of dissolved inorganic carbon in seawater, *Mar. Chem.*, *76*(4), 271–283, doi:10.1016/s0304-4203(01)00067-6.

Johannessen, S. C., W. L. Miller, and J. J. Cullen (2003), Calculation of UV attenuation and colored dissolved organic matter absorption spectra from measurements of ocean color, *J. Geophys. Res.*, *108*(C9), 3301, doi:10.1029/2000jc000514.

Kaiser, K., and R. Benner (2012), Characterization of lignin by gas chromatography and mass spectrometry using a simplified CuO oxidation method, *Anal. Chem.*, *84*, 459–464, doi:10.1021/ac202004r.

Kieber, D. J., J. McDaniel, and K. Mopper (1989), Photochemical source of biological substrates in sea water: Implications for carbon cycling, *Nature*, *341*, 637–639, doi:10.1038/341637a0.
Lenes, J. M., B. P. Darrow, C. Cattrall, C. A. Heil, M. Callahan, G. A. Vargo, R. H. Byrne, J. M. Prospero, D. E. Bates, and K. A. Fanning (2001), Iron fertilization and the Trichodesmium response on the West Florida shelf, *Limnol. Oceanogr.*, *46*(6), 1261–1277.
Lohrenz, S., W.-J. Cai, X. Chen, and M. Tuel (2008), Satellite assessment of bio-optical properties of northern Gulf of Mexico coastal waters following hurricanes Katrina and Rita, *Sensors*, *8*(7), 4135–4150, doi:10.3390/s8074135.
Lohrenz, S. E., G. L. Fahnenstiel, D. G. Redalje, G. A. Lang, M. J. Dagg, T. E. Whitledge, and Q. Dortch (1999), Nutrients, irradiance, and mixing as factors regulating primary production in coastal waters impacted by the Mississippi River plume, *Cont. Shelf Res.*, *19*(9), 1113–1141.
Louchouarn, P., S. Opsahl, and R. Benner (2000), Isolation and quantification of dissolved lignin from natural waters using solid-phase extraction and GC/MS, *Anal. Chem.*, *72*(13), 2780–2787.
Mannino, A., M. E. Russ, and S. B. Hooker (2008), Algorithm development and validation for satellite-derived distributions of DOC and CDOM in the U.S. Middle Atlantic Bight, *J. Geophys. Res.*, *113*, C07051, doi:10.1029/2007JC004493.
Meyers-Schulte, K. J., and J. I. Hedges (1986), Molecular evidence for a terrestrial component of organic matter dissolved in ocean water, *Nature*, *321*, 61–63.
Mopper, K., and D. J. Kieber (2002), *Biogeochemistry of Marine Dissolved Organic Matter*, edited by D. A. Hansell and C. A. Carlson, pp. 456–509, Academic, San Diego, Calif.
Morey, S. L., P. J. Martin, J. J. O'Brien, A. A. Wallcraft, and J. Zavala-Hidalgo (2003), Export pathways for river discharged fresh water in the northern Gulf of Mexico, *J. Geophys. Res.*, *108*(C10), 3303, doi:10.1029/2002JC001674.
Mulholland, M. R., P. W. Bernhardt, C. A. Heil, D. A. Bronk, and J. M. O'Neil (2006), Nitrogen fixation and release of fixed nitrogen by Trichodesmium spp. in the Gulf of Mexico, *Limnol. Oceanogr. Methods*, *51*(4), 1762–1776.
Ohlmann, J. C., and P. P. Niiler (2005), Circulation over the continental shelf in the northern Gulf of Mexico, *Prog. Oceanogr.*, *64*(1), 45–81.
Ohlmann, J. C., P. P. Niiler, C. A. Fox, and R. R. Leben (2001), Eddy energy and shelf interactions in the Gulf of Mexico, *J. Geophys. Res.*, *106*(C2), 2605–2620, doi:10.1029/1999jc000162.
Opsahl, S., and R. Benner (1997), Distribution and cycling of terrigenous dissolved organic matter in the ocean, *Nature*, *386*, 480–482.
Ortner, P. B., T. N. Lee, P. J. Milne, R. G. Zika, M. E. Clarke, G. P. Podesta, P. K. Swart, P. A. Tester, L. P. Atkinson, and W. R. Johnson (1995), Mississippi River flood waters that reached the Gulf Stream, *J. Geophys. Res.*, *100*(C7), 13,595–13,601, doi:10.1029/95JC01039.
Qian, T., A. Dai, and K. E. Trenberth (2007), Hydroclimatic Trends in the Mississippi River Basin from 1948 to 2004, *J. Clim.*, *20*(18), 4599–4614, doi:10.1175/jcli4262.1.
Sathyendranath, S. (2000), Remote sensing of ocean colour in coastal, and other optically-complex, Waters, *Rep. 3*, 140 pp., Int. Ocean Colour Coord. Group, Dartmouth, Canada.
Schiller, R. V., V. H. Kourafalou, P. Hogan, and N. D. Walker (2011), The dynamics of the Mississippi River plume: Impact of topography, wind and offshore forcing on the fate of plume waters, *J. Geophys. Res.*, *116*, C06029, doi:10.1029/2010JC006883.
Schilling, K. E., K.-S. Chan, H. Liu, and Y.-K. Zhang (2010), Quantifying the effect of land use land cover change on increasing discharge in the Upper Mississippi River, *J. Hydrol.*, *387*(3–4), 343–345, doi:10.1016/j.jhydrol.2010.04.019.
Shen, Y., C. G. Fichot, and R. Benner (2012), Floodplain influence on dissolved organic matter export from the lower Mississippi-Atchafalaya River system to the Gulf of Mexico, *Limnol. Oceanogr. Methods*, *57*(4), 1149–1160, doi:10.4319/lo.2012.57.4.1149.
Smith, S. V., and J. T. Hollibaugh (1993), Coastal metabolism and the oceanic organic-carbon balance, *Rev. Geophys.*, *31*(1), 75–89.
Stone, G. W., N. D. Walker, A. Hsu, A. Babin, B. Liu, B. D. Keim, W. Teague, D. Mitchell, and R. Leben (2005), Hurricane Ivan's Impact along the northern Gulf Of Mexico, *Eos Trans. AGU*, *86*(48), 497–501, doi:10.1029/2005eo480001.
Stubbins, A., R. G. M. Spencer, H. Chen, P. G. Hatcher, K. Mopper, P. J. Hernes, V. L. Mwamba, A. M. Mangangu, J. N. Wabakanghanzi, and J. Six (2010), Illuminated darkness: Molecular signatures of Congo River dissolved organic matter and its photochemical alteration as revealed by ultrahigh precision mass spectrometry, *Limnol. Oceanogr.*, *55*, 1467–1477, doi:10.4319/lo.2010.55.4.1467.
Tehrani, N., E. D'Sa, C. Osburn, T. Bianchi, and B. Schaeffer (2013), Chromophoric dissolved organic matter and dissolved organic carbon from Sea-Viewing Wide Field-of-View Sensor (SeaWiFS), Moderate Resolution Imaging Spectroradiometer (MODIS) and MERIS sensors: Case study for the Northern Gulf of Mexico, *Remote Sens.*, *5*(3), 1439–1464, doi:10.3390/rs5031439.
Torres, M. A., M. P. Barros, S. C. G. Campos, E. Pinto, S. Rajamani, R. T. Sayre, and P. Colepicolo (2008), Biochemical biomarkers in algae and marine pollution: A review, *Ecotoxicol. Environ. Safety*, *71*(1), 1–15, doi:10.1016/j.ecoenv.2008.05.009.
Vukovich, F. M. (2012), Changes in the Loop Current's Eddy shedding in the period 2001–2010, *Int. J. Oceanogr.*, *2012*, 18, doi:10.1155/2012/439042.
Walker, N. D., O. K. Huh, L. J. Rouse, and S. P. Murray (1996), Evolution and structure of a coastal squirt off the Mississippi River delta: Northern Gulf of Mexico, *J. Geophys. Res.*, *101*(C9), 20,643–20,655, doi:10.1029/96JC00919.
Walker, N. D., W. J. Wiseman, L. J. Rouse, and A. Babin (2005), Effects of River discharge, wind stress, and slope eddies on circulation and the satellite-observed structure of the Mississippi River Plume, *J. Coastal Res.*, 1228–1244, doi:10.2112/04-0347.1.
Xie, H., S. Bélanger, G. Song, R. Benner, A. Taalba, M. Blais, J. É. Tremblay, and M. Babin (2012), Photoproduction of ammonium in the southeastern Beaufort Sea and its biogeochemical implications, *Biogeosciences*, *9*(8), 3047–3061, doi:10.5194/bg-9-3047-2012.
Yuan, J., R. L. Miller, R. T. Powell, and M. J. Dagg (2004), Storm-induced injection of the Mississippi River plume into the open Gulf of Mexico, *Geophys. Res. Lett.*, *31*, L09312, doi:10.1029/2003gl019335.
Zhang, X., M. Marta-Almeida, and R. D. Hetland (2012a), A high-resolution pre-operational forecast model of circulation on the Texas-Louisiana continental shelf and slope, *J. Oper. Oceanogr.*, *5*(1), 19–34.
Zhang, X., R. D. Hetland, M. Marta-Almeida, and S. F. DiMarco (2012b), A numerical investigation of the Mississippi and Atchafalaya freshwater transport, filling and flushing times on the Texas-Louisiana Shelf, *J. Geophys. Res.*, *117*, C11009, doi:10.1029/2012JC008108.